Electronic Supplementary Material (ESI) for Nanoscale
This journal is © The Royal Society of Chemistry 2014

Supplementary Information for:

Temprature Driven Assembly of Like-Charged Nanoparticles at a Liquid-Liquid and Liquid-Air Interface[†]

Qiang Zhuang[‡], David A. Walker[‡], Kevin P. Browne, Bartlomiej Kowalczyk, and Bartosz A. Grzybowski*

S1 Synthesis and Film Deposition

S1.1 – Synthesis of Au Nanoparticles:

Spherical AuNPs functionalized with FMP were synthesized using a seed mediated growth procedure and subsequent ligand exchange similar to that outlined by Peng and co-workers.[33] Dodecyl amine (DDA) stabilized 2 nm seed particles were synthesized by injecting 5.7 mL of a 80 mM (117 mg) tetrabutylammonium borohydride (TBAB) and 84 mM (222 mg) dilauryldimethylammonium bromide (DDAB) toluene solution into a 13.2 mL toluene solution of 9 mM $HAuCl_4 \cdot 3H_2O$ (47 mg), 182 mM DDA (444 mg), and 91 mM DDAB (554 mg) under vigorous stirring. This solution was stirred at room temperature overnight before further use. The seeds were then added to 113.4 mL of a toluene growth solution (8.8 mM $HAuCl_4 \cdot 3H_2O$, 0.25 M DDA and 40 mM DDAB; 446 mg, 5.248 g and 2.095 g, respectively). 43.8 mL of toluene solution contianing 0.1 M DDAB (2.095 g) and 0.2 M anhydrous hydrazine (290 mg) was added drop-wise over the course of 30 minutes to the aforementioned growth/seed mixture under vigorous stirring. This solution was allowed to age and ripen overnight to create 5.8±0.4 nm gold nanoparticles stabilized by DDA/DDAB.

S1.2 – Synthesis of FMP Ligand:

Unless otherwise stated, all solvents and reagents were used from commercial sources without further purification. Analytical thin-layer chromatography was performed using 250 µm fluorescent silica gel glass plates (Sigma-Aldrich) and visualized with UV irradiation (254 nm) or I_2 staining. Flash-chromatography was performed on high-purity grade, 200-400 mesh silica gel (Sigma-Aldrich). Nuclear magnetic resonance (NMR) spectra were recorded on a Bruker Avance III 500 MHz spectrometer, with working frequencies of 499.373 for ^1H and 125.579 MHz for ^{13}C nuclei, respectively. Chemical shifts are reported in ppm and referenced to the residual non-deuterated solvent frequencies; for $CDCl_3$ δ 7.26 for ^1H and δ 77.1 for ^{13}C; for d_6-DMSO δ 2.50 for ^1H and δ 39.5 for ^{13}C; for CD_3CN δ 1.94 for ^1H and δ 1.32 for ^{13}C. Mass spectra were recorded on a Thermo Finnigan LCQ Advantage ESI mass spectrometer.

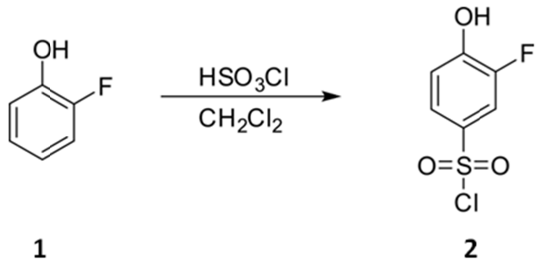

Sulfonyl chloride 2. This compound was prepared according to a previous literature synthesis.[33] Briefly, chlorosulfonic acid (14.3 mL, 214 mmol, 6 eq.) was added dropwise to a solution of fluorophenol **1** (Sigma-Aldrich; 4.0 g, 35.7 mmol, 1 eq.) in CH_2Cl_2 (40 mL) at room temperature. The mixture was then heated at reflux for 3 hours while stirring with magnetic stir bar. The mixture was then allowed to cool to room temperature, and the lower (orange) layer was poured into a separatory funnel containing ~ 100 mL crushed ice (*caution: pour* *slowly*). The aqueous solution was then acidified with HCl and was extracted with diethyl ether (3 x 100 mL). The ether extractions were set aside and the aqueous layer was saturated with NaCl, followed by extraction with diethyl ether (3 x 100 mL). The ether layers were combined, dried over $MgSO_4$, and the solvent was evaporated, leaving an orange residue. The crude compound **2** was used without further purification.

2 **3**

Monofluorothiophenol 3. This compound was prepared according to a previous literature synthesis.[33] Briefly, crude sulfonyl chloride **2** (1.11 g, 5.27 mmol, 1 eq.) was added to 4.6 M H_2SO_4 (aq.; 14 mL) and the solution was cooled to 0 °C. Zn powder (s; 1.72 g, 5 eq.) was then added in portions with continuous stirring, and stirring continued at room temperature for 1 hr. The mixture was then heated at reflux for 4 hr. Once cold, the solvent was evaporated and was directly adsorbed onto silica gel and was purified by column chromatography (silica gel, CH_2Cl_2–hexanes – ethyl acetate–MeOH, 45/33/17/5, *v*/*v*/*v*/*v*), yielding the pure compound (0.72 g, 14% over 2 steps). NMR: δ_H(500 MHz, CD_3CN, 298 K) 7.50 (1 H, s, SH), 7.25 (1 H, d, $J_{1,3}$ 10.9 Hz, Ph-H), 7.13 (1 H, d, $J_{1,3}$ 9.0 Hz, Ph-H), 6.93 (1 H, t, $J_{1,3}$ 9.0 Hz, Ph-H); δ_C(125 MHz, CD_3CN, 298K) 152.0 (d, $J_{1,1}$ 243.5 Hz), 146.0 (d, $J_{1,2}$ 14.1 Hz), 128.4 (d, $J_{1,3}$ 3.62 Hz), 128.2 (d, $J_{1,2}$ 6.4 Hz), 119.3 (s), 119.2 (d, $J_{1,3}$ 2.1 Hz); MS (EI) *m/z* ($[M\cdot MeOH]^-$) 175.

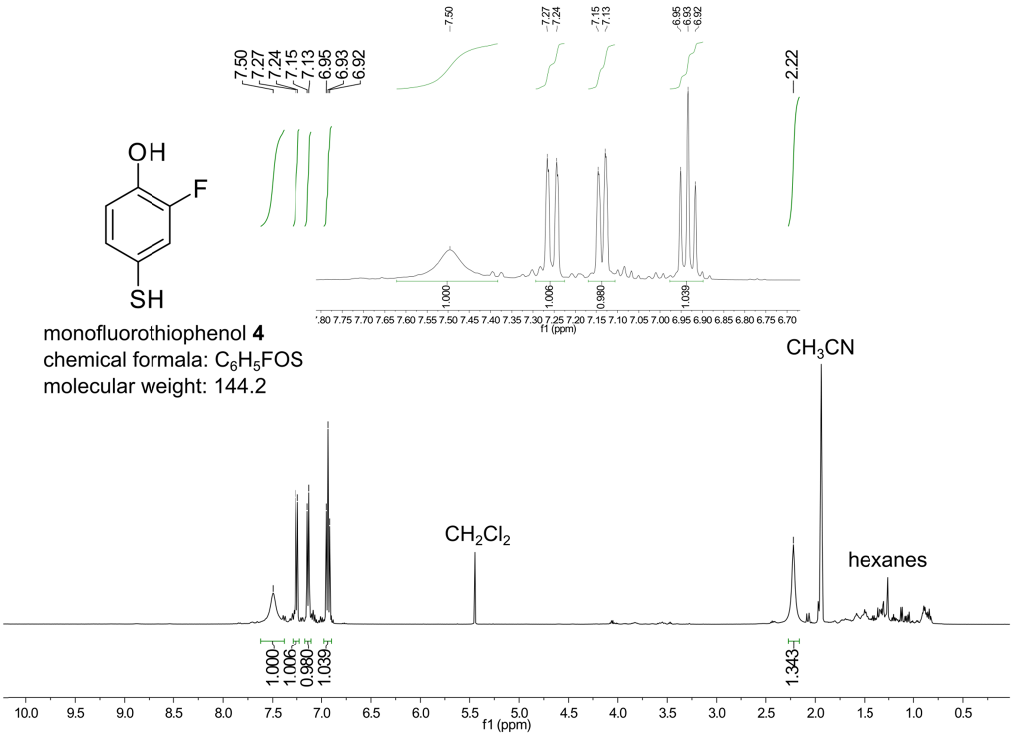
OH
F
SH
monofluorothiophenol 4
chemical formala: C6H5FOS
molecular weight: 144.2
7.50
7.27
7.24
7.15
7.13
6.95
6.93
6.92
2.22
1.000
1.006
0.980
1.039
1.343
CH3CN
CH2Cl2
hexanes
f1 (ppm)
10.0 9.5 9.0 8.5 8.0 7.5 7.0 6.5 6.0 5.5 5.0 4.5 4.0 3.5 3.0 2.5 2.0 1.5 1.0 0.5
7.80 7.75 7.70 7.65 7.60 7.55 7.50 7.45 7.40 7.35 7.30 7.25 7.20 7.15 7.10 7.05 7.00 6.95 6.90 6.85 6.80 6.75 6.70

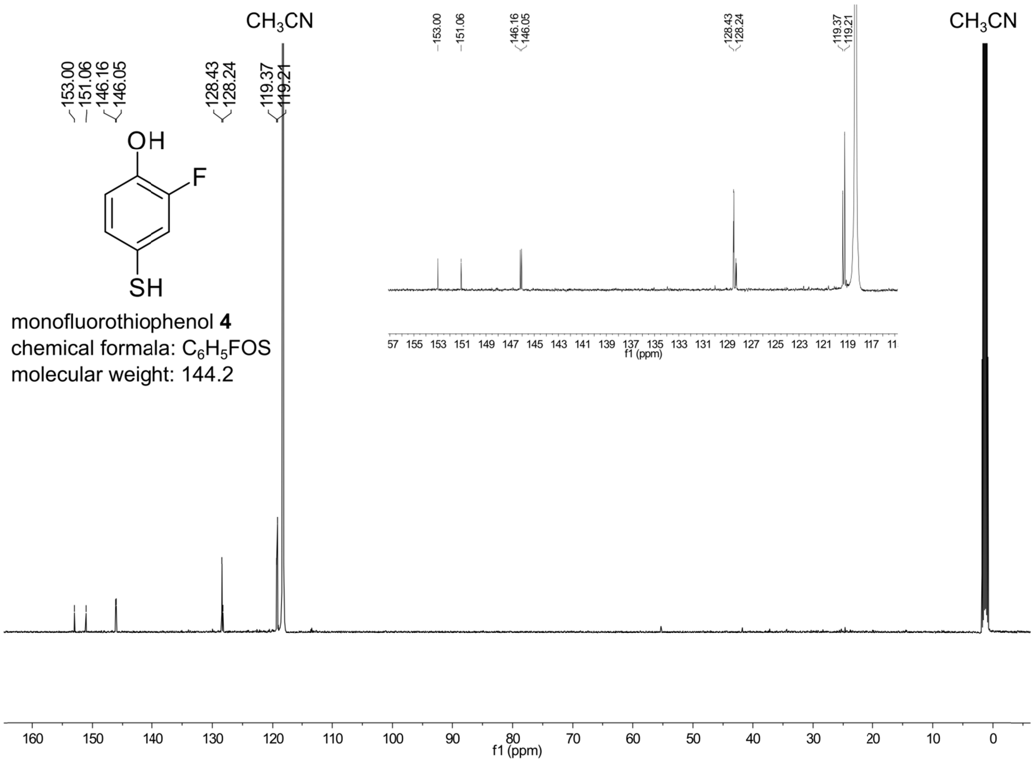
OH
F
SH
monofluorothiophenol 4
chemical formala: C6H5FOS
molecular weight: 144.2
153.00
151.06
146.16
146.05
128.43
128.24
119.37
119.21
CH3CN
CH3CN
f1 (ppm)
160 150 140 130 120 110 100 90 80 70 60 50 40 30 20 10 0
57 155 153 151 149 147 145 143 141 139 137 135 133 131 129 127 125 123 121 119 117 11

S1.3 – Functionalization of Au Nanoparticles:

To functionalize the toluene based AuNPs with FMP, 50 mL of the 5.8 nm AuDDA/DDAB particles were quenched with 50 mL of methanol to induce their precipitation. After allowing the aggregates to sediment (~1 hr after flocculation), the clear supernatant of toluene/methanol containing excess DDA and DDAB surfactant was removed. The particles were briefly dried over argon flow (to remove all traces of methanol) and then immediately redispersed in 50 mL of toluene. To this mixture, a concentrated aliquot of FMP ligand dissolved in toluene was immediately added (0.4 equivalents of ligand per gold atom, ~36 mg). The ligands were allowed to age overnight, allowing the formation of a high quality SAM, and then the NPs were precipitated with ~50 mL of acetone (this precipitation can be facilitated by the addition of tetramethylammonium hydroxide, TMAOH, base if necessary). After allowing the aggregates to sediment, the solids were washed three times with 20 mL of dichloromethane (to remove remaining surfactants and excess FMP ligand). The final product was briefly dried using a flow of argon gas (to remove any trace of acetone/DCM) and then dissolved in DI water adjusted to pH~9 for film formation experiments and pH~10.5 for long term storage by addition of base (tetramethylammonium hydroxide, TMAOH). To remove any larger aggregates that might have formed during the purification process, the aqueous solution was passed through a 200 nm syringe filter.

S1.4- Formation of NP Films at Droplet Interfaces:

In our experiments, the pH of the AuFMP NP solution was adjusted to ~9. The concentration of NPs was ~60 mM in the terms of gold atoms. To illustrate the temperature driven film formation, a droplet of 5 uL AuFMP NPs solution was immersed in the mixture of toluene and dichloromethane (3:1 *v*:*v*) in a vial. The organic phase was then cooled down by placing the vial into a acetone/dry ice bath. After 3 ~5 minutes, the NPs migrated to the interface between water and organic solvent and formed the metalized film. Simultaneously, water inside the droplets began to freeze. Next, the dry ice bath was removed and the frozen droplet began to melt, revealing a shiny, metallic film.

NPs functionalized with FMP were kinetically stable in aqueous solutions with a pH above 9.5. When the pH was commensurate with the pK$_a$ prior to the freeze-thaw cycle (e.g. pH=9.5 at 25^{o}C), any significant excess NPs for which there was not sufficient interfacial area to occupy ($[\mathrm{NP}]V_{droplet}\pi r^2 / \mathrm{N}_{\mathrm{Avagadro}} >> \text{Interfacial Area}$) aggregated in solution during the freeze-thaw cycle. This aggregation was observed as a blue-shift in the NPs' surface plasmon resonance recorded by UV-Vis spectroscopy (Figure S2a). On the other hand, when the pH≫pKa (e.g., pH~11) the NPs will remain stable in solution regardless of changes in temperature, as indicated by the lack of a blue-shift in the NPs' surface plasmon resonance following a freeze-thaw cycle (Figure S2b).

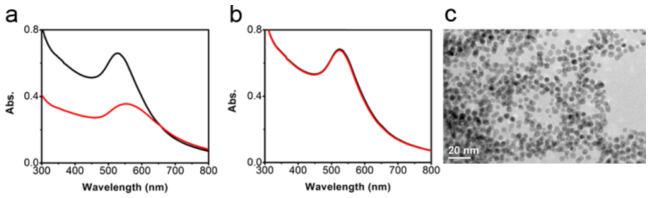

Figure S1 (a) The UV-Vis spectra of FMP nanoparticle solution before (black line) and after (red line) a freeze-thaw cycle which began at pH = 9.5 when at 25 ^{o}C. **(b)** The UV-Vis spectra of FMP nanoparticle solution before (black line) and after (red line) a freeze-thaw cycle which began at pH = 11 when at 25 ^{o}C. **(c)** The TEM image of FMP functionalized nanoparticles

S1.5 – Wet Stamping of NP Films:

1 wt% agarose film: 0.3 g agarose was dispersed in 29.7 g DI water. The agarose suspension was heated in a microwave for ~1 min. The clear solution was then poured onto a pre-heated glass slide. The other pre-heated glass slide was placed on top of the gel. The gel was then allowed to cool down, producing and agarose film for stamping experiments.

3 wt% agarose stamps: 1.5 g agarose was dispersed in 48.5 g DI water. The suspension was heated in a microwave for about 1.5 min and was then cast over a photolithographically-prepared polydimethylsiloxane (PDMS) master presenting the "negative" of the desired microfeatures on its surfaces. The agarose-covered PDMS was then placed under vacuum for about 2 min to remove any air bubbles. After the agarose layer cooled down and solidified, it was gently peeled-off the master and cut into smaller stamps.

NPs Stamping: Aagarose stamps were soaked into a ~60 mM AuFMP nanoparticle solution overnight. After blotting off any surface water with a tissue paper, the stamps was placed onto the agarose substrate and left there for 1 hr under humid (100% RH) atmosphere. Finally, the stamp was removed and the gold NP films were formed on the surface by decreasing the temperature of the agarose film as described in the main text.

S2 Electrostatic Modeling & Interfacial Energies

S2.1 – Describing the Behavior of Electrostatic Potential:

For the experimental conditions described in this work, the electrostatic potential, φ, outside of the particles is well described by the full Poisson Boltzmann (PB) equation simplified for monovalent electrolytes.

$$\nabla^2\varphi = \frac{2\mathrm{e}^2 c_s}{\varepsilon_\mathrm{o}\varepsilon}\sinh\left(\frac{\mathrm{e}\varphi}{\mathrm{k_B}T}\right) \tag{1}$$

The introduction of the dimensionless electrostatic potential, $\psi = \mathrm{e}\varphi/\mathrm{k_B}T$, results in the equation below characterized by a single parameter κ^2.

$$\nabla^2\psi = \frac{2\mathrm{e}^2 c_s}{\varepsilon_\mathrm{o}\varepsilon\mathrm{k_B}T}\sinh(\psi) = \kappa^2\sinh(\psi) \tag{2}$$

Here, $\kappa^{-1} = \left(2\mathrm{e}^2 c_s/\varepsilon_\mathrm{o}\varepsilon\mathrm{k_B}T\right)^{-1/2}$ is the Debeye screening length which characterizes the behavior of the system and is approximately the length scale over which the potential decays away from charged surfaces. The PB equation (2) can also be used to describe the potential decay within the alkane SAM, although one must account for the differences in dielectric and ionic environment ($\varepsilon \approx 2$ for an alkane SAM). Within the metallic nanoparticle core, the potential must be constant – this can be approximated by assuming the 'dielectric constant' of the metal is much greater than the dielectric constant of the surrounding environment ($\varepsilon_\mathrm{Au}/\varepsilon_\mathrm{water} \to \infty$) such that the PB equation simplifies to the Laplace equation, $\nabla^2\psi = 0$, within the nanoparticle core.

S2.2 – Describing the Charged Particle Interface:

In order to accurately describe the experimental system, the boundary conditions for the nanoparticle-solvent interface must incorporate as much experimental detail as possible. While purely analytical solutions exist for 'constant-potential' or 'constant-charge' boundary conditions, these assumptions fail to capture the complex equilibrium between the SAM and surrounding counterions and cannot be applied to this particular system. Consequently, we turn to what is known as the 'charge-regulation' boundary condition which is typically solved numerically due to the coupling of non-linear differential equations. In this method, the charge density, σ, at the interface of the SAM and the solvent is described by the grafting density of all chemical moieties, Γ, multiplied by the fraction, γ, of those groups which are in a charged state based on the local chemical and electrical equilibrium at the interface.

For the 'charge regulating' boundary condition, the charge density for a flat SAM is described as $\sigma = ze\Gamma\gamma$, where e is the elementary charge, *z* is the valence of the charged moieties and Γ is the density of bound moieties on the surface $\Gamma_o = 4.47$ligands/nm for a flat <111> gold surface). Transforming the equation into a non-dimensional form yields:

$$\bar{\sigma} = \frac{ze}{\varepsilon\varepsilon_o k_B T}\Gamma\gamma \tag{3}$$

To extend this definition of charge density to a spherical particle, one must take into account the effective "dilution" of charge density on the surface by the curvature of the particle. The apparent charge density at the SAM-solvent interface is described as $\Gamma = \Gamma_o r_{NP}^2 / (r_{NP} + l)^2$, where Γ_o is the ligand density on a flat surface, r_{NP} is the radius of the nanoparticle core, and *l* is the thickness of the SAM.

At any given time, the surface of the charged NP is in electro-chemical equilibrium with the surrounding medium. The charge regulation boundary condition accounts for this and defines the actual charge density at the interface to be a fraction, γ, of the total possible charge density. For a moiety A^-H^+ in the presence of B^+ counter-ions, this fraction can be defined as

$$\gamma = \frac{C^s_{A^-}}{C^s_{Total}} = \frac{C^s_{A^-}}{C^s_{A^-} + C^s_{AH} + C^s_{AB}} = \frac{1}{1 + C^s_{AH}\big/C^s_{A^-} + C^s_{AB}\big/C^s_{A^-}} \tag{4}$$

where $C^s_{A^-}$ is the concentration of deprotonated A^-H^+ at the surface, C^s_{Total} is the total concentration of ligands on the surface, C^s_{AH} is the concentration of deprotonated A^-H^+ at the surface, and C^s_{AB} is the concentration of A^- at the surface that has absorbed the counterion, B^+. The adsorption of protons and counterions onto the charged surface can be related to the bulk concentrations through the following equations derived through a series of mass balances:

$$\frac{C^s_{AH}}{C^s_{A^-}} = \frac{C^o_{H^+}}{K_a}\exp(-\psi) \tag{5}$$

$$\frac{C^s_{AB}}{C^s_{A^-}} = X^o_{B^+}\exp\left(\frac{\Delta G_d}{k_B T} - \psi\right) \tag{6}$$

where $C^o_{H^+}$ is the bulk concentration of H^+, K_a is the disassociation coefficient of the acid, $X^o_{B^+}$ is the mole fraction of B+ in the bulk solution, and ΔG_d is the Gibb's free energy for the disassociation of the A^+B^- complex.

Combining the original equation for charge density, (3), with the corrections for curvature and chemical equilibrium, (4), yields equation (7) which can be applied at the SAM-solvent interface.

$$\bar{\sigma} = \frac{ze\Gamma_o}{\varepsilon\varepsilon_o k_B T}\frac{r_{NP}^2}{(r_{NP}+l)^2}\frac{1}{\left(1 + \exp(-\psi)\left(C^o_{H^+}\big/K_a + X^o_{B^+}\exp\left(\Delta G_d\big/k_B T\right)\right)\right)} \tag{7}$$

S2.3 – COMSOL FEM Solver and Calculating Free Energies of Interaction:

While analytical solutions exist for the more simplistic constant charge and constant potential boundary conditions, the charge regulating boundary condition is best solved numerically unless one is to make a series of simplifying assumptions. In order to solve the above described equations we used a finite element method (FEM) solver, COMSOL v.4.2 (formerly known as FEMLAB). Prior to applying the FEM solver to the our specific problem, the solver was calibrated by solving the simple scenario of two interacting spheres of constant surface potential for which it was found to be in agreement with the analytical solution (to within less than 1%).

Having established the accuracy of the numerical solver, the potential profile of a single nanoparticle and for two interacting nanoparticles at separation *h* was solved. The free energy of each system was calculated by integrating the forces across the particles' surfaces[2, 34], as described by equation (8) for small values of ψ

$$\bar{F} = \frac{F}{\mathrm{k_B}T} = -\left(\frac{\varepsilon\varepsilon_\mathrm{o}\mathrm{k_B}T}{2\mathrm{e}^2}\right)\int\int_0^{\Psi_o} \bar{\sigma}\, d\psi\, ds \approx -\int \bar{\sigma}\psi \big/ 2\, ds \tag{8}$$

where $\bar{F}$ is the dimensionless free energy and Ψ_o is the equilibrium dimensionless surface potential of the particles. The electrostatic interaction energies between particles were calculated through equation (9), where *i* and *ii* correspond to the configurations shown in Figure S2a and S2b, respectively.

$$U_{es} = \Delta\bar{F} = \bar{F}_i - 2\bar{F}_{ii} \tag{9}$$

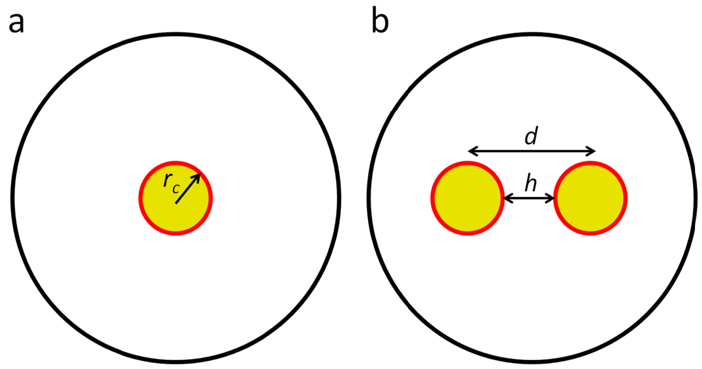

Figure S2: Geometries for (a) a single and (b) two interacting particles at separation *h* as calculated in the FEM solver.

S2.4 – Calculation of van der Waals Interactions and Total Energies of Interaction:

In traditional Derjaguin, Landau, Verwey, and Overbeek (DLVO) theory, the total interaction energies between particles can be obtained by simply summing up energies of interactions of infinitesimal elements on each particle. In our system, there is a competition between two contributing forces – repulsion through electrostatics and attraction though van der Waals (vdW) interactions.

The vdW interactions can be described through analytical means by applying the Hamaker approximation. For two spherical particles, the vdW interaction energies can be described as

$$U_{vdW} = -\frac{A}{3}\left[\frac{r_c^2}{d^2 - 4r_c^2} + \frac{r_c^2}{d^2} + \frac{1}{2}\ln\left(1 - \frac{4r_c^2}{d^2}\right)\right] \tag{10}$$

where A is the Hamaker coefficient for the pertinent media (in this case, gold across water A ≈ 4×10^{-20}J), r_c is the radius of the nanoparticle core, and d is the distance between the centers of the two nanoparticles (see Figure S2b).

The total energy of particles' interaction can be described as a sum:

$$U_{total} = U_{es} + U_{vdW} \tag{11}$$

As can be seen in Figure 2a of the main text, the total interaction energy is negative (i.e. attractive) at very small distances but there is an energy barrier due to the electrostatic interactions that prevents the nanoparticles from approaching one another and aggregating. As the temperature lowers, and consequently the pH of the solution lowers, the energy barrier preventing aggregation is weakened and at a critical temperature, T_c, the nanoparticles begin to aggregate and form an insoluble film at the interface of the two liquid phases.

S2.5 – Free Energy of Interfacial Adsorption:

The free energy associated with a NP adsorbing onto a liquid-liquid interface has been previously discussed at length by Stebe and co-workers[26]. The gain in free energy comes from the reduction of interfacial area (the cross section of the NP) between two immiscible solvents which have a high surface tension. A simple free energy balance of the surfaces coupled with the Young-Dupré equation results in the following equation:

$$\Delta F_{ads} = -\gamma_{12}\pi r_{NP}^2\left(1\text{-}\cos\theta\right)^2 \tag{12}$$

where γ_{12} is the surface tension between the two fluid phases, r_{NP} is the radius of the NP and θ is the contact angle between the three-phase interface (solvent 1, solvent 2, and the NP surface).

In the current FMP NP system, measuring the three-phase contact angle can be accomplished by measuring the contact angle of sessile droplets on FMP SAMs formed on flat Au surfaces. Gold slides were prepared by thermally evaporating a 2 nm tungsten adhesion layer and 50 nm of 99.999% gold at 1Å/s onto glass slides. The slides were then placed into a 20 mM MeOH solution of FMP molecules and allowed to incubate for at least 24 hours. To prepare the SAM for contact angle measurements, the slide was first rinsed with MeOH and then acetone and blown dry with pressurized argon gas. At this stage, the slide was placed in a 2mM buffer (pH 4 phthalate buffer; pH 7 phosphate buffer; pH 10 carbonate buffer) solution at the pH for which the measurement were to be performed. After equilibrating for 5 minutes, the slide was removed from the buffer solution and excess water was blown off of the slide using pressurized argon; the slide was then immediately placed into the a solution of interest (here a toluene/DCM mixture). A Sessle droplet of the 2 mM buffer solution was placed on the SAM and contact angle was measured. Multiple contact angles (~60) were taken for different droplets at a given pH. In between different pH measurements, the slide was returned to the MeOH FMP solution and allowed to re-equilibrate for at least 6 hours – this ensures that the SAMs are returned to their original state.

pH	Buffer/Organic Contact Angle	Buffer/Air Contact Angle
4	$141.23^{o} \pm 2.8^{o}$	$75.6^{o} \pm 3.1^{o}$
7	$140.55^{o} \pm 3.0^{o}$	$73.85^{o} \pm 2.3^{o}$

10	$128.48^{\circ} \pm 2.3^{\circ}$	$67.95^{\circ} \pm 3.3^{\circ}$

S3 Dependence between pH and temperature

The pH of aqueous solutions is influenced by atmospheric gasses which dissolve into water (e.g., CO_2). Although the concentration of CO_2 in the air is only ~0.03%, the pH of the DI water can be significantly lowered when this minute fraction of CO_2 dissolves in water. In principle, the solubility of CO_2 in water is a decreasing function of temperature. It depends on: the $CO_2(aq) + H_2O \leftrightarrow H_2CO_3$ equilibrium and can be quantified by the Henry's law. Although $[CO_2(aq)]$ is larger than $[H_2CO_3]$, $[H_2CO_3]$ still can be substituted for all the dissolved $CO_2(aq)$. Based on the equilibriums, mass conversation and electric neutrality, pH can be calculated by the following equations:

$$K_o = \frac{c_{CO_2}}{P_{CO_2}} \tag{13}$$

Where the P_{CO2} is the partial pressure of CO_2 in air, K_o is the solubility in mol L^{-1} atm^{-1}, and c is the concentration of CO_2 dissolved in the water:

$$c_{CO_2} = \left[H_2CO_3\right] + \left[HCO_3^-\right] + \left[CO_3^{2-}\right] \tag{14}$$

H_2CO_3 dissociates in water as $CO_2(aq) + H_2O \leftrightarrow HCO_3^- + H^+$ and $HCO_3^- \leftrightarrow CO_3^{2-} + H^+$ such that the corresponding equilibrium coefficients are:

$$K_1 = \frac{\left[HCO_3^-\right]\left[H^+\right]}{\left[H_2CO_3\right]} \tag{15}$$

$$K_2 = \frac{\left[CO_3^{2-}\right]\left[H^+\right]}{\left[HCO_3^-\right]} \tag{16}$$

Based on the electric neutrality of the solution,

$$\left[H^+\right] + \left[TMA^+\right] = \left[HCO_3^-\right] + 2\left[CO_3^{2-}\right] + \left[OH^-\right] \tag{17}$$

Where the $[TMA^+]$ comes from the base that is added to the solution to adjust pH.

$$K_w = \left[OH^-\right]\left[H^+\right] \tag{18}$$

Where K_w is the dissociation constant of water.

Moreover, all the dissociation constants here are functions of temperature and can be expressed as described by Harned and co-authors[35]:

$$pK_o = -\frac{2622.38}{T} - 0.0178471T + 15.5873 \tag{20}$$

$$pK_1 = \frac{3404.71}{T} - 0.032786T - 14.8425 \tag{21}$$

$$\mathrm{pK}_2 = \frac{2902.39}{T} + 0.02379T - 6.4980 \tag{22}$$

$$\ln\left(\mathrm{K}_\mathrm{w}\right) = 148.9802 - \frac{13847.26}{T} - 23.6521\ln\left(T\right) \tag{23}$$

Finally, by solving all the equations above for the pH at specific temperatures, we receive a trend that agrees with the experimental results as show in Figure 1b in the main text.

References

33. M. Sato, Y. Kawashima, J. Goto, Y. Yamane, Y. Chiba, S. Jinno, M. Satake and C. Iwata, Eur. J. Med. Chem., 1995, 30, 403.
34. K. J. M. Bishop, C. E. Wilmer, S. Soh and B. A. Grzybowski, Small, 2009, 5, 1600.
35. H. S. Harned and R. Davis, J. Am. Chem. Soc., 1943, 65, 2030.